JOURNAL OF ELECTROMAGNETIC ENGINEERING AND SCIENCE, VOL. 17, NO. 3, 113~119, JUL. 2017

http://dx.doi.org/10.5515/JKIEES.2017.17.3.113
ISSN 2234-8395 (Online) · ISSN 2234-8409 (Print)

Application of Compressive Sensing to Two-Dimensional Radar Imaging Using a Frequency-Scanned Microstrip Leaky Wave Antenna

(*Invited Paper*)

Shang-Te Yang · Hao Ling*

Abstract

The application of compressive sensing (CS) to a radar imaging system based on a frequency-scanned microstrip leaky wave antenna is investigated. First, an analytical model of the system matrix is formulated as the basis for the inversion algorithm. Then, L_1-norm minimization is applied to the inverse problem to generate a range-azimuth image of the scene. Because of the antenna length, the near-field effect is considered in the CS formulation to properly image close-in targets. The resolving capability of the combined frequency-scanned antenna and CS processing is examined and compared to results based on the short-time Fourier transform and the pseudo-inverse. Both simulation and measurement data are tested to show the system performance in terms of image resolution.

Key Words: Compressive Sensing, Leaky Wave Antenna, Near Field, Radar Imaging, Resolution.

I. INTRODUCTION

Compressive sensing (CS) is an emerging signal processing technique based on L_1-norm minimization. CS has been applied to two-dimensional (2D) radar imaging to reduce both the number of frequencies and the number of antenna elements (or the number of spatial samples in the case of a synthetic aperture) required for data collection [1–6]. The frequency and element positions are randomized to overcome aliasing in the downrange and grating lobes in the radiation pattern, respectively. In this paper, we explore the use of CS for 2D range-azimuth radar imaging. However, we explore a unique application in which CS is applied to an imaging system based on a frequency-scanned antenna.

A frequency-scanned antenna is a low-cost alternative to a linear phased-array system for obtaining 2D range-azimuth information of targets in a scene. The beam of a frequency-scanned antenna can be steered to different directions by changing the carrier frequency. At the same time, there is still sufficient bandwidth during beam dwell on the target to obtain range information. Consequently, a scene can be imaged with one single frequency sweep. This concept was exploited earlier in [7, 8]. More recently, we have designed, built, and tested a frequency-scanned microstrip leaky wave antenna (MLWA) to track humans [9]. Image formation was performed using the short-time Fourier transform (STFT). Targets are first resolved in range by using a range-gated sliding window. The range-gated response is then Fourier-transformed into the frequency domain, in which target angular information can be obtained. However, the choice of the window function leads to a tradeoff

Manuscript received June 10, 2017 ; Accepted July 11, 2017. (ID No. 20170610-024J)
Department of Electrical and Computer Engineering, The University of Texas at Austin, Austin, TX 78712, USA.
*Corresponding Author: Hao Ling (e-mail: ling@ece.utexas.edu)

in the range and azimuth resolution.

The problem of generating a 2D image from a single frequency response collected using a frequency-scanned antenna can alternatively be approached by considering this problem as a solution to a highly underdetermined system of linear equations. The image domain is a large 2D space, and the measured data is the 1D frequency response. Therefore, the imaging problem is well-suited for CS, that is, how to generate a large but sparse 2D image from a compressed 1D frequency response. Because only a few moving targets are expected within the scene of interest, a solution can be effectively determined by using L_1-norm minimization. Some related preliminary results were reported in [9].

In this paper, we investigate in detail the application of CS to a 2D radar imaging system based on a frequency-scanned antenna. We develop the system matrix based on the antenna characteristics, range delay, and a point-scatterer target model. We then apply L_1-norm minimization to generate the 2D range-azimuth image. The present study is novel in several respects compared to our earlier study in [9]. First, the antenna is a new, narrow-beam antenna that we have designed specifically for operation with a short-pulse radar [10]. It has a length of 90 cm (approximately three times longer than the design reported in [9]), operates between 3 and 6 GHz, and is capable of a beamwidth of the order of 5°. Accordingly, additional near-field considerations are needed to property model the system matrix for applying CS. Second, we closely examine the resolving capability of the combined frequency-scanned radar and CS processing. Both simulation and measurement data are tested to show the system performance in terms of image resolution and to clarify whether the combined system can operate beyond the physical resolution limit.

The remainder of this paper is organized as follows. Section II describes the performance of the long MLWA and discusses the far- and near-field CS formulations. In Section III, we examine the resolution of the combined system based on simulation and measurement. Section IV presents the conclusions of this study.

II. MLWA AND CS FORMULATION

The antenna under consideration is a 90-cm-long, air-filled, half-width MLWA. Fig. 1 shows the built prototype, and the inset shows its cross-sectional dimensions. The antenna is designed to operate from 3 to 6 GHz. Fig. 2 shows the gain pattern of the antenna versus the frequency and angle as simulated using the FEKO electromagnetic simulation software [11]. An infinitely large ground plane is used in the simulation. The gain value is color coded from 0 to 20 dBi. The horizontal axis is the angle θ, which is defined with respect to the longitudinal z-

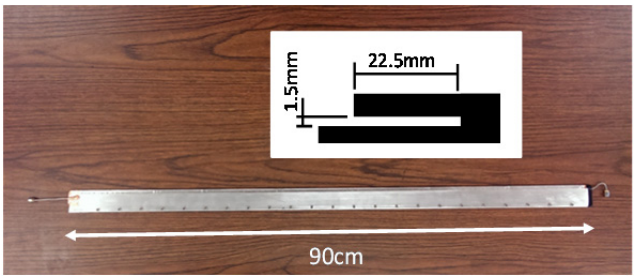

Fig. 1. Photograph of the built 90-cm-long MLWA. The inset shows its cross-sectional dimensions.

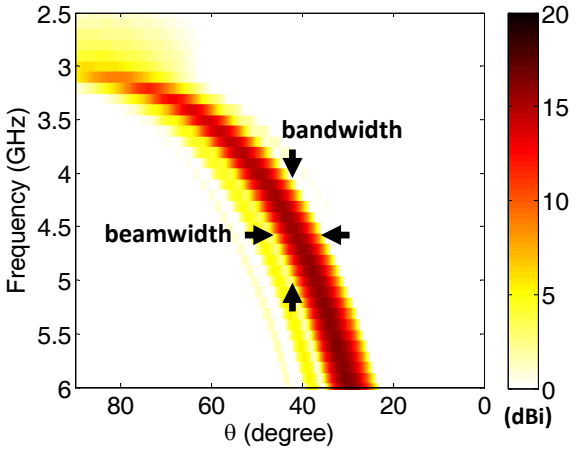

Fig. 2. Simulated gain pattern of the 90-cm-long MLWA as a function of frequency and angle.

direction of the antenna. As the frequency is increased, the antenna beam sweeps from the broadside direction ($\theta = 90°$) toward the endfire direction ($\theta = 0°$), with increasing peak gain. The beamwidth of the antenna is marked by the horizontal arrows in Fig. 2, and it is a function of the beam direction. Similarly, we can define a "target illumination bandwidth" by a vertical cut across the pattern, as shown in the figure. This quantity dictates the achievable range resolution for radar imaging. The tracking of humans using this antenna in combination with a short-pulse radar and STFT processing was reported in [10]. An investigation into further narrowing the beamwidth of the antenna can be found in [12].

To apply CS, we formulate the 2D imaging problem into an underdetermined system of linear equations as follows:

$$\mathbf{y} = \mathbf{A}\mathbf{x} = \sum_{i=1}^{N} \mathbf{a}_i x_i \tag{1}$$

where $\mathbf{x}$ is the large but sparse 2D range-azimuth image, and $\mathbf{y}$ is the measured frequency response. If we neglect the interaction between targets, we can express $\mathbf{y}$ as a superposition of the frequency responses from point targets at different positions. Therefore, x_i, the i-th element of the $\mathbf{x}$ vector, is the strength of a target located at position (R_i, θ_i), and $\mathbf{a}_i$, the i-th column vector of the $\mathbf{A}$ matrix, denotes the corresponding direction-dependent

frequency response of a target with unity strength in the 2D range-azimuth plane. $\mathbf{a}_i$ contains both the antenna response and a free-space propagation factor, and it can be written as follows:

$$\mathbf{a}_i = \left(E^{ff}(f,\theta_i) \cdot \frac{e^{-jk_0 R_i}}{R_i} \right)^2 \tag{2}$$

where $k_0 = 2\pi f/c$. $E^{ff}(f, \theta)$ is the frequency-dependent far-field of the MLWA. The square accounts for the two-way propagation. We next model $E^{ff}(f, \theta)$ as the radiation from an equivalent magnetic line source on the narrow antenna aperture along the z-direction as follows:

$$E^{ff}(f,\theta) = \frac{-jk_0}{2\pi}\sin(\theta)\int_0^L e^{(-\alpha-j\beta)z} \cdot e^{+jk_0\cos(\theta)\cdot z}\, dz \tag{3}$$

where $L = 0.9$ m is the antenna length. α and β are respectively the attenuation and propagation constant of the leaky mode. They can be computed approximately using the transverse resonance method (TRM) [13].

The above CS formulation is based on the far-field radiation pattern of the antenna. However, the far-field distance of the 90-cm-long antenna at 6 GHz is 32.4 m based on the $2L^2/\lambda$ criterion. To properly account for close-in targets, a more exact near-field $\mathbf{a}_i$ can also be formulated as follows:

$$\mathbf{a}_i = \left[\frac{-jk_0}{2\pi}\int_0^L \sin(\theta(z)) \cdot e^{(-\alpha-j\beta)z} \cdot \frac{e^{-jk_0 R(z)}}{R(z)} dz \right]^2 \tag{4}$$

where $R(z)$ and $\theta(z)$ are respectively the distance and direction of a near-field target to different parts on the antenna aperture. This equation simplifies to (2) and (3) when the far-field approximation $R(z) = R_i - z\cos(\theta_i)$ is applied. Computing the $\mathbf{A}$ matrix using the more exact (4) requires carrying out aperture integration repeatedly for every possible target position across the entire 2D range-azimuth plane.

We first test the far-field CS formulation with simulated data from a 3 × 3 grid of point targets. The ground truth is shown in Fig. 3(a). The downrange locations of the targets are 31, 33, and 35 m. The azimuth directions are 37°, 53°, and 67°. Based on the target map, a frequency response $\mathbf{y}$ is generated using the more exact numerical integration shown in (4). However, the matrix $\mathbf{A}$ is generated by using the far-field approximation in (2) and (3). The MATLAB package YALL1 [14] is used to solve the L_1-norm minimization with linear constraints, and the resulting image is shown in Fig. 3(b). It is seen that the downrange and azimuth positions of the targets are resolved correctly. The model mismatch between the more exact $\mathbf{y}$ vector and the far-field $\mathbf{A}$ matrix is not severe.

Next, the nine targets are moved to 4, 6, and 8 m with the same azimuth positions. The corresponding CS image is shown in Fig. 3(c). It can be observed that the azimuth positions of the close-in targets are not correctly located and that the target response is more diffused. This is due to the model mismatch between the far-field $\mathbf{A}$ matrix and the target response vector $\mathbf{y}$.

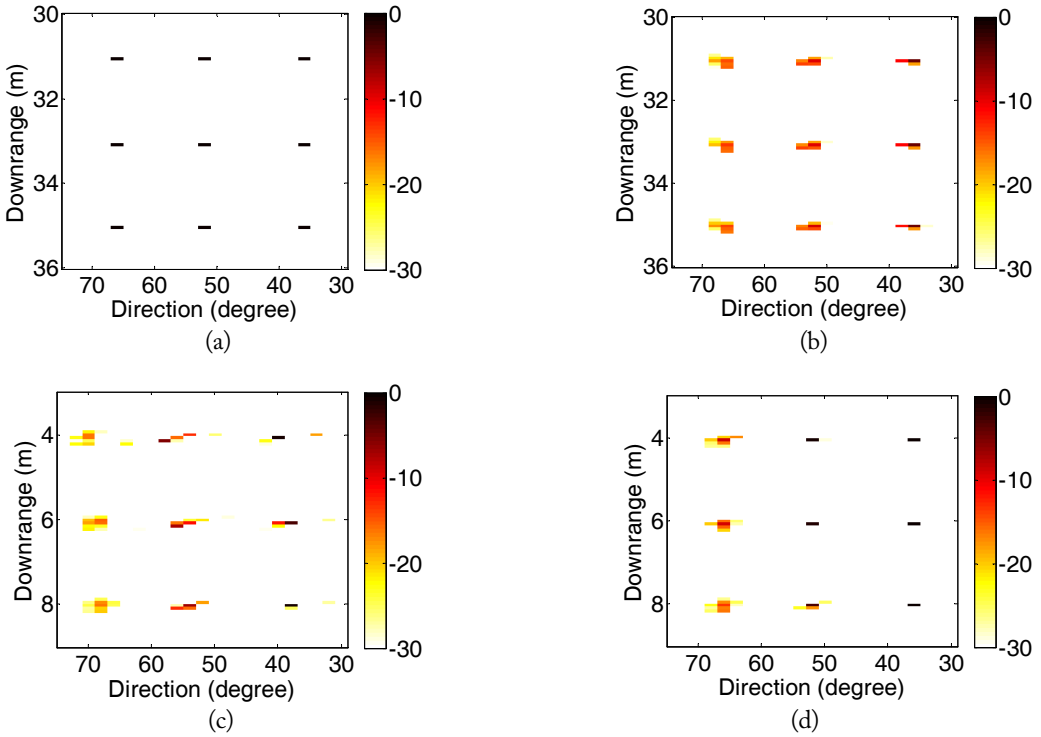

Fig. 3. Testing of far- and near-field formulations. (a) Ground truth map of 3×3 point targets located far away from the antenna. (b) CS image generated using the far-field $\mathbf{A}$. (c) CS image of close-in targets generated using the far-field $\mathbf{A}$. (d) CS image of close-in targets generated using the near-field $\mathbf{A}$.

The same targets are then imaged using the near-field **A** matrix, and the resulting image is shown in Fig. 3(d). In comparison to Fig. 3(c), all the targets are now better focused and the azimuth positions are restored correctly. It is noted that although the targets near the broadside direction are better focused compared to Fig. 3(c), they are still blurrier than the other targets in Fig. 3(d). This could be due to the broader antenna beam near the broadside direction. Lastly, targets are better focused in Fig. 3(d) than in Fig. 3(b), indicating that the minor error introduced by the far-field approximation still degrades the performance of CS. Therefore, it is worthwhile to incorporate as much sensor physics as possible when performing CS imaging. For the remainder of this paper, the near-field **A** matrix computed using (4) is used.

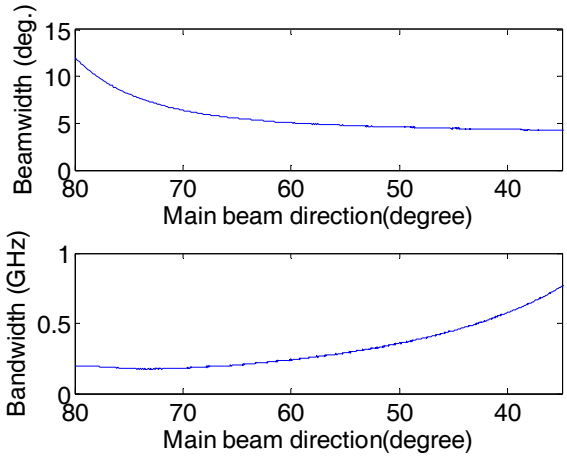

Fig. 4. Two-way 3-dB antenna beamwidth and 3-dB frequency bandwidth of 90-cm-long MLWA. They are plotted as functions of the beam direction.

III. Resolving Capability Study

To examine the resolving capability of the combined CS-MLWA system, closely spaced targets are imaged. For conventional Fourier-based imaging, the azimuth resolving capability is the 3 dB beamwidth of the antenna, and the downrange resolution is inversely proportional to the 3 dB frequency bandwidth. Fig. 4 shows the beamwidth and frequency bandwidth of the 90-cm-long antenna. The same antenna is used for both transmitting and receiving; thus, the 3 dB beamwidth shown in Fig. 4 is based on the square of the gain pattern to account for two-way radiation/reception. It should be noted that the beamwidth and bandwidth are both functions of the beam direction. The beamwidth is approximately 5° for most of the target directions, and the bandwidth ranges from 200 to 750 MHz. Correspondingly, the Fourier resolutions in range, based on the $c/2/bandwidth$ formula, are 75 and 20 cm, respectively. Three groups of three closely spaced targets are placed at approximately $\theta = 40°$, 55°, and 70° to evaluate the direction-dependent resolving capability. Fig. 5(a) shows the ground truth image. The spacing between the targets in azimuth is set to one beamwidth, and the spacing in downrange corresponds to two times

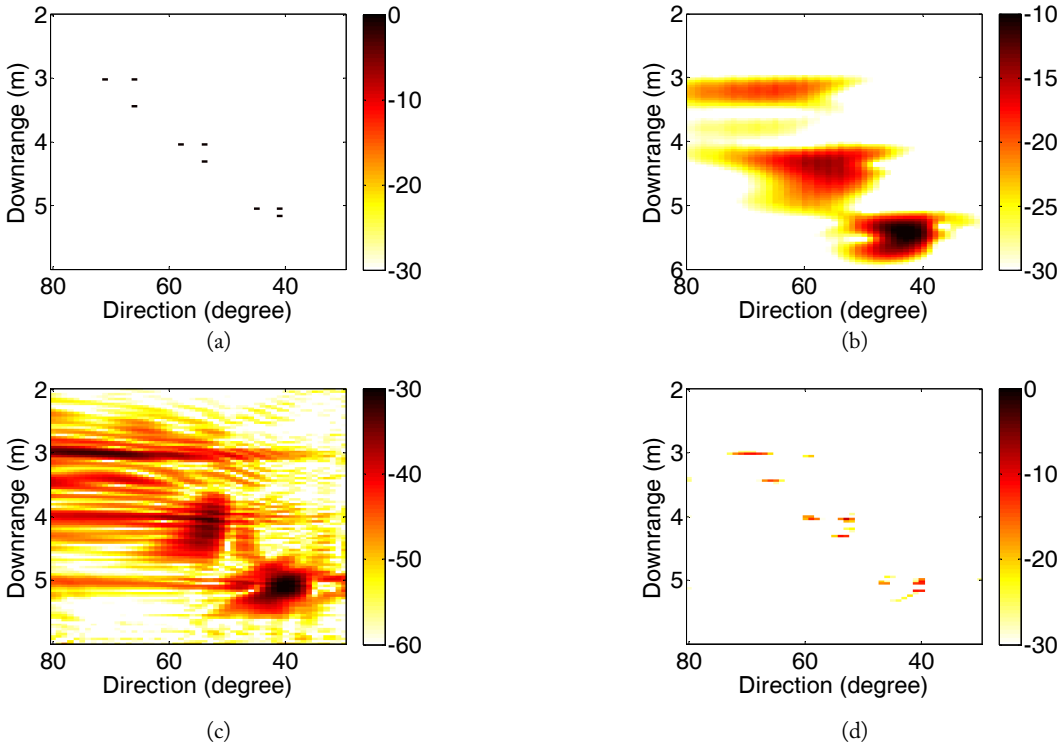

Fig. 5. Testing of target-resolving capability. (a) Ground truth map of three groups of targets spaced by their direction-dependent resolutions. (b) Image generated using STFT. (c) Image generated using a pseudoinverse. (d) Image generated using CS.

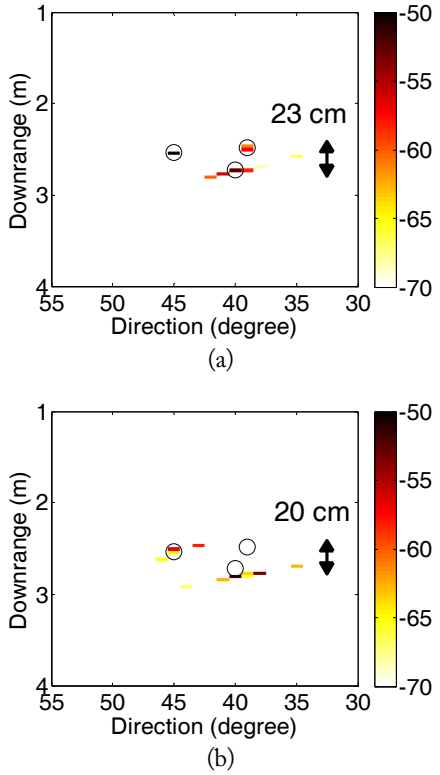

Fig. 6. CS images of three trihedrals measured using the MLWA. (a) Image showing three resolved targets. (b) Image showing only two resolved targets when the farthest trihedral is moved 3 cm closer.

the bandwidth or one-half of the Fourier range resolution. All targets are set to unity strength. As was done in Section III, a frequency response is simulated based on Eq. (4) and a point-scatterer model.

The frequency response is first processed using STFT with a 50-cm sliding Hamming window; the result is plotted in Fig. 5(b). STFT barely resolves targets in downrange, and it cannot resolve targets in the azimuth dimension. It should also be noted that the downrange locations of the targets are not correct, because the direction-dependent group delay of the leaky mode is not modeled by STFT. Next, the pseudoinverse of the near-field **A** matrix is used to generate the image shown in Fig. 5(c). The result is equivalent to solving the underdetermined system of linear equations with L_2-norm minimization. It is observed that targets are better resolved in downrange. Moreover, the targets in the farthest group (at approximately 5 m in downrange) are marginally resolved in azimuth. However, there are substantial artifacts, and it is very difficult to identify the true targets. Lastly, Fig. 5(d) shows the image generated using the near-field **A** matrix and YALL1.

Eight of the nine targets are resolved correctly. Only the target at ($R = 3$ m, $\theta = 66°$) is not shown correctly. Because the targets are placed based on the far-field beamwidth, the two closest-in targets could be spaced too closely to be resolved properly by the near-field beam. Among the three different algorithms, CS achieves the best 2D resolution in the range-azimuth plane. Moreover, it appears that CS can slightly surpass the Fourier resolution in the downrange dimension. More testing revealed that CS could not correctly resolve targets placed closer than one beamwidth, showing that the azimuth resolution is still governed by the physical aperture of the antenna.

Finally, measurement data are collected, and the resolving capability of the system is tested using three trihedrals. A vector network analyzer is used as a radar to collect S_{11} of the antenna in the presence of trihedrals from 2 to 6 GHz. A background subtraction is performed to remove the antenna mismatch and room clutter. During the measurement, the azimuth and downrange spacings between the trihedrals are progressively reduced until just before the trihedrals can no longer be resolved in the corresponding CS image. The result is plotted in Fig. 6(a), where the CS-generated image is shown in color, and the actual target locations are overlaid on the image as open circles. The two targets on the right with roughly the same azimuth position are placed with a 23-cm difference in downrange. The azimuth spacing between the left- and the right-hand-side targets is approximately 5°. These numbers correspond approximately to the beamwidth and frequency bandwidth shown in Fig. 4 at $\theta = 39°$. Next, we move the farthest target 3 cm closer in downrange; the corresponding CS image is shown in Fig. 6(b). It is observed that one target disappears from the image. Moreover, the responses of the remaining two targets become diffused. Testing with measurement data shows that the resolving capability in the azimuth dimension agrees with that found from testing with simulation data. However, we were not able to achieve super-resolution in downrange in the measurement data testing. This could be attributed to several reasons, including mismatch between the TRM-predicted radiation pattern and the built prototype, mismatch between the backscattering from the actual trihedral (18 cm per side) and the point target assumption, and higher-order interactions between targets.

IV. Conclusion

In this paper, the application of CS to 2D radar imaging using a frequency-scanned antenna has been investigated. First, an analytical model of the system matrix was formulated as the basis for the inversion algorithm. Then, L_1-norm minimization was applied to the inverse problem to generate the image of the scene. It was found that because of the antenna length, a near-field formulation is needed to properly image close-in targets. The resolution of the system was then tested rigorously by using closely spaced targets that were placed based on the direction-dependent beamwidth and bandwidth of the frequency-scanned

antenna. It was found that CS achieves the best image resolution in the range-azimuth plane when compared to STFT and a pseudoinverse. Nevertheless, the image resolution achievable using CS is limited by the physical antenna beamwidth in the azimuth dimension and the frequency bandwidth in the downrange dimension. Although the simulations showed some superresolution performance in the downrange dimension, it was not confirmed in the measurement. This could be due to secondary effects not modeled in our formulation, including the actual target response, interactions between targets, and mismatch between the actual antenna prototype and the modeled system matrix. This highlights the importance of accounting for as much of the sensor physics as possible to achieve good performance in terms of image resolution when applying CS.

This work was supported by the Texas Norman Hacerman Advanced Research Program under Grant No. 003658-0065-2009 and the National Science Foundation under Grant No. ECCS-1232152.

REFERENCES

[1] L. C. Potter, E. Ertin, J. T. Parker, and M. Cetin, "Sparsity and compressed sensing in radar imaging," *Proceedings of the IEEE*, vol. 98, no. 6, pp. 1006–1020, 2010.

[2] L. Carin, D. Liu, and B. Guo, "Coherence, compressive sensing, and random sensor arrays," *IEEE Antennas and Propagation Magazine*, vol. 53, no. 4, pp. 28–39, 2011.

[3] L. Zhang, Z. J. Qiao, M. Xing, Y. Li, and Z. Bao, "High-resolution ISAR imaging with sparse stepped-frequency waveforms," *IEEE Transactions on Geoscience and Remote Sensing*, vol. 49, no. 11, pp. 4630–4651, 2011.

[4] E. Lagunas, M. G. Amin, F. Ahmad, and M. Najar, "Joint wall mitigation and compressive sensing for indoor image reconstruction," *IEEE Transactions on Geoscience and Remote Sensing*, vol. 51, no. 2, pp. 891–906, 2013.

[5] L. Poli, G. Oliveri, and A. Massa, "Microwave imaging within the first-order Born approximation of the contrast-field Bayesian compressive sensing," *IEEE Transactions on Antennas and Propagation*, vol. 60, no. 6, pp. 2865–2879, 2012.

[6] N. Whitelonis and H. Ling, "High-resolution radar imaging through a pipe via MUSIC and compressed sensing," *IEEE Transactions on Antennas and Propagation*, vol. 61, no. 6, pp. 3252–3260, 2013.

[7] W. Mayer, M. Wetzel, and W. Menzel, "A novel direct-imaging radar sensor with frequency scanned antenna," in *Proceedings of 2003 IEEE MTT-S International Microwave Symposium Digest*, Philadelphia, PA, 2003, pp. 1941–1944.

[8] Y. Alvarez-Lopez, C. Garcia, C. Vazquez-Antuna, S. Ver-Hoeye, and F. Las Heras Andres, "Frequency scanning based radar system," *Progress in Electromagnetics Research*, vol. 132, pp. 275–206, 2012.

[9] S. T. Yang and H. Ling, "Application of a microstrip leaky wave antenna for range-azimuth tracking of humans," *IEEE Geoscience and Remote Sensing Letters*, vol. 10, no. 6, pp. 1384–1388, 2013.

[10] S. T. Yang and H. Ling, "Combining a frequency-scanned antenna and a short-pulse radar for 2-D imaging," in *Proceedings of 2014 IEEE Antennas and Propagation Society International Symposium (APSURSI)*, Memphis, TN, 2014, pp. 137-138.

[11] EM Software & Systems Inc. FEKO version 6.3. Stellenbosch, South Africa: EM Software & Systems Inc., 2013.

[12] S. T. Yang and H. Ling, "Two-section half-width microstrip leaky wave antenna," *IEEE Transactions on Antennas and Propagation*, vol. 62, no. 10, pp. 4988–4996, 2014.

[13] G. M. Zelinski, G. A. Thiele, M. L. Hastriter, M. J. Havrilla, and A. J. Terzouli, "Half width leaky wave antennas," *IET Microwaves, Antennas & Propagation,* vol. 1, no. 2, pp. 341–348, 2007.

[14] J. Yang and Y. Zhang, "Alternating direction algorithms for l_1 problems in compressive sensing," *SIAM Journal on Scientific Computing*, vol. 33, no. 1, pp. 250–278, 2011.

Shang-Te Yang

received his B.S. degree in Electrical Engineering from National Taiwan University, Taipei City, Taiwan in 2006. He received the M.S. and Ph.D. degrees in Electrical Engineering from the University of Texas at Austin, Austin, TX, USA, in 2011 and 2014, respectively. In August 2014, he joined Apple Inc. in Cupertino, CA. His research interests include frequency-scanned antennas, radar signal processing, low-complexity radar systems, and time-varying radar signatures.

Hao Ling

received his B.S. degrees in Electrical Engineering and Physics from Massachusetts Institute of Technology, Cambridge, MA, USA, in 1982, and his M.S. and Ph.D. degrees in Electrical Engineering from the University of Illinois at Urbana-Champaign, Urbana, IL, USA, in 1983 and 1986, respectively. He joined the faculty of the University of Texas at Austin, Austin, TX, USA, in 1986 and was Professor of Electrical and Computer Engineering and holder of the L. B. Meaders Professorship in Engineering. He retired from the University of Texas in January 2017. Dr. Ling's principal areas of research have been in radar signature prediction and radar feature extraction. He has actively contributed to the development and validation of numerical and asymptotic methods for characterizing the radar signatures from complex targets. In 1986, he and his collaborators pioneered the shooting and bouncing ray (SBR) technique for predicting the radar returns from realistic aerospace vehicles. He was a co-developer of the SBR-based code Xpatch, which has been distributed to over 450 government and industrial organizations in the United States. His recent research interests also include radar signal processing, radar sensing of humans, miniaturized and broadband antenna design, and propagation channel modeling in non-line-of-sight environments. He has published over 200 journal papers and 230 conference papers and coauthored a book on radar imaging (Norwood, MA: Artech House, 2002). Dr. Ling received the NSF Presidential Young Investigator Award in 1987, the NASA Certificate of Appreciation in 1991, and the University of Illinois Distinguished Alumni Award in 2009. From 2015 to 2017, he served as a Program Director in the Electrical, Communications, and Cyber Systems Division at the US National Science Foundation, where he managed a program in communications and sensing. He has been an Associate Editor of the *IEEE Transactions on Antennas and Propagation* since 2013. He is a Fellow of IEEE.